Growth Mechanisms of Anisotropic Layered Group IV Chalcogenides on van der Waals Substrates for Energy Conversion Applications

Peter Sutter[1,*] and Eli Sutter[2]

[1]Department of Electrical and Computer Engineering, University of Nebraska-Lincoln, Lincoln, NE 68588, United States; [2]Department of Mechanical and Materials Engineering, University of Nebraska-Lincoln, Lincoln, NE 68588, United States

Abstract

Two-dimensional group IV monochalcogenide semiconductors (SnX, GeX; X = S, Se) are of fundamental interest due to their anisotropic crystal structure and predicted unique characteristics such as very large exciton binding energies and multiferroic order possibly up to above room temperature. Whereas growth on reactive supports produces mostly standing flakes, deposition on van der Waals (vdW) substrates can yield basal-plane oriented layered crystals. But so far, this approach invariably resulted in flakes that are several atomic layers thick and the synthesis of monolayers has remained elusive. Here, we use *in-situ* microscopy during molecular beam epitaxy of SnS on graphite and graphene to establish the origin of this predominant multilayer growth. The enhanced reactivity of group IV chalcogenide layers causes adsorption of precursor molecules primarily on the initial SnS nuclei instead of the vdW support. On graphite, this unusual imbalance in the material supply is the primary cause for fast vertical growth. Experiments on graphene/Ru(0001) suggest increased adsorption on the vdW substrate, which enables enhanced lateral SnS growth. The fundamental insight obtained here provides a basis for identifying conditions for the scalable synthesis of single-layer group IV monochalcogenides, and guides the growth of high-quality multilayer films of interest for applications in energy conversion, optoelectronics, and thermoelectrics.

*Corresponding author, e-mail: psutter@unl.edu.

Keywords: Semiconductor, 2D crystal, low-energy electron microscopy, adsorption, van der Waals growth, anisotropy.

Introduction

Group IV monochalcogenides (SnX, GeX; X: S, Se) are anisotropic layered/2D crystals representing compound analogues of black phosphorus/phosphorene.[1] In bulk form, these materials have long been considered for energy conversion applications (*e.g.*, thin film photovoltaics)[2-7] and have shown other exceptional characteristics such as record thermoelectric performance.[8] Recent theoretical calculations have predicted a number of intriguing properties for single-layer group IV monochalcogenides, including very large exciton binding energies (up to 0.7 eV) in GeS and SnS,[9-10] high carrier mobility,[11] strain-tunable band offsets and charge separation in lateral GeS-SnS heterostructures,[12] selective valley polarization,[13] and ferroelectricity/ferroelasticity up to above room temperature,[13-16] which in conjunction with bandgaps in the visible or near infrared spectral range may enable the facile coupling between electromagnetic radiation and multiferroic order.[17]

To access these predicted properties in the ultrathin limit and pave the way for applications of this family of 2D semiconductors, robust approaches toward monolayer group IV chalcogenides are required. In contrast to other 2D materials, the successful mechanical exfoliation of monolayer SnS or SnSe has not been reported to date. The transformation of SnS_2 by introduction of sulfur vacancies, e.g., by irradiation with high energy electrons,[18-19] can produce ultrathin SnS, albeit with limited domain size. Bottom-up growth has been hindered by two challenges: (i) achieving uniform basal-plane orientation; and (ii) limiting vertical growth to obtain single-layer (2D) films. On reactive supports (*e.g.*, transition metals or oxides) SnS and related materials grow in the form of multilayer nanoflakes that couple to the substrate edge-on at random tilt angles.[20-23] Basal-plane oriented growth can be achieved by suppressing covalent edge bonding of initial nuclei to the substrate surface, *e.g.*, by growth on van der Waals (vdW) supports. Previous work showed the growth of basal-plane oriented SnS

(or SnSe) on different substrates including SiO_2,[24] NaCl,[25] as well as mica[26-28] and graphene[29-30] van der Waals supports. In growth from SnO_2 and S powders on SiO_2, the crystal phase could be tuned between SnS_2 and SnS by varying the substrate temperature.[24] SnS flakes formed epitaxially on NaCl substrates.[25] Highly textured, basal-plane oriented SnS with different thickness and in-plane shapes resulted from growth on mica and graphene van der Waals substrates. However, the reported growth processes invariably resulted in thicker multilayer flakes, which points to fundamental mechanisms that cause pronounced vertical (out-of-plane) growth and thus hinder the bottom-up synthesis of ultrathin group IV monochalcogenides.

Here, we use *in-situ* low-energy electron microscopy (LEEM) during molecular beam epitaxy (MBE) of SnS to identify the growth mechanisms of basal-plane oriented few-layer group IV monochalcogenide semiconductors on two types of van der Waals (vdW) substrates: highly oriented pyrolitic graphite, and monolayer graphene on Ru(0001). Our results confirm a strong tendency toward multilayer growth found in previous work, which makes the scalable synthesis of ultrathin (monolayer) SnS challenging. By analyzing time-resolved *in-situ* microscopy data obtained during growth we identify an unusually high surface reactivity of group IV monochalcogenides as the origin of this competition between desired lateral and parasitic vertical growth. In addition, our experiments show distinct growth phenomena of layered crystals, including rapid lateral grain growth and distinct avenues for introducing crystal defects such as dislocations, which have no analogues in conventional three-dimensional (3D) materials but strongly affect the growth of 2D and layered crystals. Our results can guide the identification of conditions suitable for controlled bottom-up synthesis of ultrathin group IV chalcogenide crystals and have important implications for the growth of

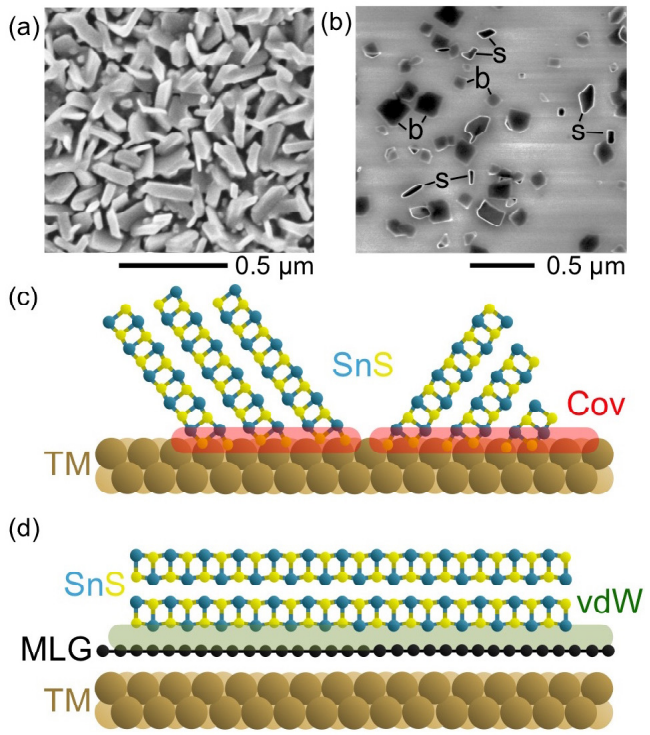

Figure 1: Growth of layered group IV chalcogenides on metals. (a) Scanning electron micrograph (SEM) of SnS grown on Au/SiO_2 at 300°C. Nearly all SnS flakes are standing at different angles. **(b)** SEM of SnS grown on SiO_2/Si at 300°C. Examples of standing and basal-plane oriented SnS flakes are marked 's' and 'b', respectively. **(c)** Schematic morphology of layered SnS on transition metal (TM) substrate. Edge sites of randomly oriented SnS nuclei bond covalently (Cov) to the substrate. **(d)** Schematic morphology of SnS on a van der Waals (vdW) support, *e.g.*, monolayer graphene (MLG) on a transition metal.

high-quality layered crystals of these materials for energy conversion applications including thin film and bulk photovoltaics or thermoelectrics.

Results and Discussion

Figure 1 illustrates the need for nonreactive vdW substrates in the growth of basal-plane oriented SnS. On more reactive supports, including metals (*e.g.*, a thin Au film; Fig. 1a) or oxides (*e.g.*, SiO_2/Si; Fig. 1b), only part of the synthesized SnS flakes are oriented parallel to the support surface, whereas a significant fraction grows standing up at different angles relative to the substrate. These observations, which are consistent with literature reports,[20-23] suggest that covalent bonding between the flake edges and the surface atoms of the support can cause a

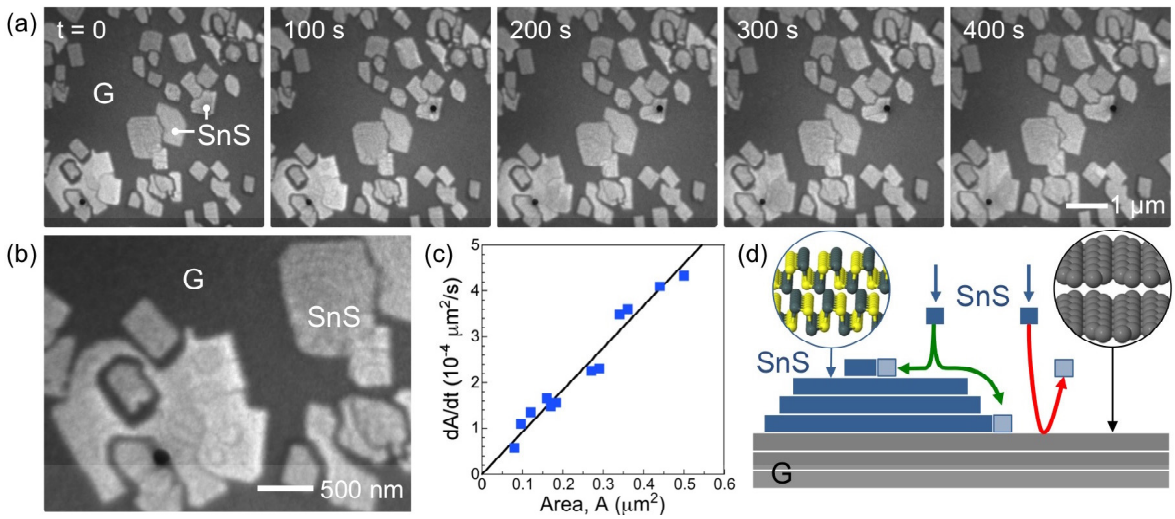

Figure 2: Real-time microscopy of SnS growth on graphite. (a) Time-lapse image sequence of LEEM images of SnS molecular beam epitaxy on graphite (G). Black spots visible in all frames (bottom left and center right) are defects in the micro-channelplate detector of our microscope. **(b)** Zoomed-in view of the SnS flakes. Faint dark lines within the flakes are atomic steps where the SnS thickness changes by one monolayer. Black spot: Detector defect. **(c)** Analysis of the SnS lateral growth rate (dA/dt) as a function of the projected flake area, A. **(d)** Schematic showing the observed predominant adsorption of SnS on existing SnS nuclei, and negligible sticking to the graphite substrate.

morphology of standing flakes (Fig. 1c). On a less reactive vdW support, this covalent edge interaction is suppressed and flakes with basal-plane orientation, *i.e.*, sheets parallel to the substrate surface, become the energetically favored configuration (Fig. 1d).

Figure 2 summarizes the analysis of real-time microscopy movies of SnS MBE growth on a clean, atomically flat graphite vdW substrate (see Supporting Information, Fig. S1) at a sample temperature of 260°C. In contrast to reactive supports, all SnS nuclei are now oriented parallel to the surface of the graphite vdW substrate, as shown schematically in Fig. 1d. However, we also observe that the lateral dimensions of the flakes remain quite small and that many of the nuclei show dark contrast along their edges, which in LEEM suggests a significant thickness. The image sequence of Fig. 2a (see also supplementary movie S1) clearly shows the lateral expansion of all SnS flakes within the field of view, and images at higher magnification (Fig. 2b) document that the flakes are crystalline and consist of planar sheets separated by single-layer high steps that are imaged as faint dark lines. To identify the origin of the observed

fast vertical growth of SnS on graphite, we analyzed the growth process from image sequences such as Fig. 2a. The results of this analysis are shown in Fig. 2c, where the rate of lateral expansion (dA/dt) is plotted against the projected area (A) of the SnS nuclei. The lateral growth rate of the SnS flakes scales linearly with their projected area, $dA/dt \sim A$, and the fitted line intersects the coordinate axes at the origin. From the linear dependence, we conclude that the SnS flakes grow predominantly by adsorption of SnS from the vapor phase directly onto their surface. In the limit $A \rightarrow 0$ the growth rate vanishes, which indicates that adsorption on the graphite surface does not contribute significantly to the SnS growth. The implications of these findings are summarized in the schematic of Fig. 2d. The SnS surface appears to be significantly more reactive than the surrounding graphite, whose sticking coefficient is negligible. Hence, adsorption on the existing SnS nuclei is by far the dominant mechanism for condensation of SnS from the vapor phase. The adsorbed SnS diffuses on the surface and contributes to both the lateral and, via nucleation of additional atomic layers, the vertical growth of the flakes. We note that this scenario is opposite to that realized in the growth of most other 2D crystals, notably graphene and boron nitride on metals,[31-32] as well as transition metal dichalcogenides on SiO_2,[33] where the surface of the growing 2D crystals is far less reactive than the surrounding substrate so that most of the adsorption – a key microscopic process not only in MBE but also in chemical vapor deposition and vapor transport growth – occurs on the support. Such predominant substrate adsorption favors lateral (2D) growth since the active growth front encountered by diffusing species is the edge of the 2D crystal, and hence nucleation of additional layers is effectively suppressed. The enhanced reactivity of SnS crystal surfaces can be traced back to the unusual electronic structure of the puckered SnS sheets. Whereas in the Sn(IV) dichalcogenide SnS_2 each Sn atom is octahedrally coordinated to

six S atoms, the Sn(II) in SnS is coordinated to three S atoms, which leaves a lone pair of electrons occupying the final tetrahedral site.[34] Besides causing enhanced surface reactivity, the interaction between these lone pair electrons on adjacent SnS sheets also gives rise to a strong interlayer interaction that has prevented the successful mechanical exfoliation of this material to monolayer thickness.[35]

To evaluate possible vdW substrates that may show enhanced SnS adsorption and hence could be more suitable for single-layer growth, we chose monolayer graphene (MLG) on Ru(0001) thin films (grown epitaxially on sapphire, see Methods). It is well established that MLG/Ru(0001) adopts a moiré structure with varying registry between the graphene sheet and

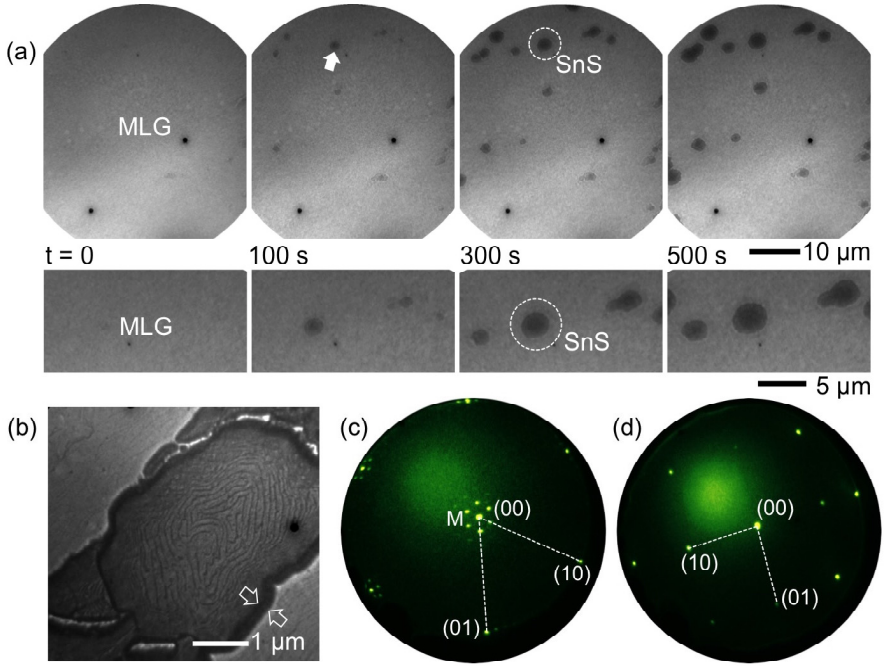

Figure 3: SnS growth on pristine, non-intercalated graphene/Ru(0001). (a) LEEM image sequence showing different stages of the growth of basal-plane oriented SnS on a monolayer graphene/Ru vdW substrate at 280°C. Note the nucleation and growth of widely spaced SnS flakes. Electron energy: ε = 5.8 eV. Black spots visible in all frames (top row, bottom left and center right) are defects in the micro-channelplate detector of our microscope. Top row: Overview images illustrating the inhomogeneous SnS nucleation. Bottom row: Part of the field of view at higher magnification. **(b)** High-magnification LEEM image showing atomic steps on a basal-plane oriented SnS island. Electron energy: ε = 2.0 eV. **(c)** Low-energy electron diffraction (LEED) pattern obtained on the MLG/Ru substrate, showing first-order [(10), (01)] spots along with characteristic moiré diffraction spots ('M'). **(d)** LEED pattern of basal-plane oriented SnS on graphene/Ru. The orthorhombic unit cell has a ratio of 1:1.1 of the (10) and (01) surface lattice constants (corresponding to *a* = 0.44 nm, *b* = 0.40 nm).

substrate lattice in a large supercell,[31] which modulates chemical reactivity and adsorption and gives rise to the selective growth of metal clusters[36] and adsorption of molecules[37-38] in specific regions of the moiré cell. This suggests that MLG/Ru may show enhanced adsorption compared to graphite. The preparation of high-quality MLG/Ru(0001) is shown in the Supporting Information (Fig. S1).[31,39-40] Exposure of clean Ru to ethylene at low pressure (5×10^{-8} Torr) at high temperature (~830°C) causes the sparse nucleation of MLG domains, which were then expanded to full surface coverage at progressively increasing C_2H_4 pressure (up to ~2×10^{-6} Torr). This procedure leaves the surface fully covered by large-domain graphene with spacing between grain boundaries exceeding 30 μm. To ensure that the MLG film formed a tight diffusion barrier against the underlying metal substrate, the ethylene exposure was continued well past the point at which LEEM showed coalescence of neighboring grains (typical additional dose: > 30 min at 2×10^{-6} Torr ≈ 3600 langmuir, L).

Figure 3 shows real-time observations during SnS deposition on this MLG/Ru vdW support. Similar to growth on graphite, SnS deposition causes nucleation and growth of SnS islands (Fig. 3a; see also supporting movie S2). For the same deposition conditions, nucleation is less dense than on graphite and the individual SnS nuclei reach substantially larger lateral sizes (up to 10 μm) before they ultimately stop expanding or coalesce to a closed film (see below). Furthermore, the SnS domains now adopt a nearly isotropic (*i.e.*, circular) growth shape in contrast to the faceted, rectangular shapes observed on graphite, which points to different mechanisms of SnS incorporation. High-magnification images of the SnS grains show clearly defined, flat layers separated by atomic steps and growth by step-attachment (Fig. 3b; see also supporting movie S3). Low-energy electron diffraction (LEED) on the substrate between SnS nuclei (Fig. 3c) shows the characteristic moiré pattern of MLG/Ru(0001) along

with first-order graphene diffraction spots.[31] Diffraction on SnS grains (Fig. 3d) shows a pattern with a characteristic rectangular unit cell with a ratio of 1:1.1 between (10) and (01) reciprocal-space vectors corresponding to real-space lattice constants a = 0.44 nm and b = 0.40 nm, confirming the formation of single-crystalline orthorhombic SnS. At increased coverage, the grains ultimately coalescence into a closed SnS film with uniform c-axis orientation (Fig. S2).

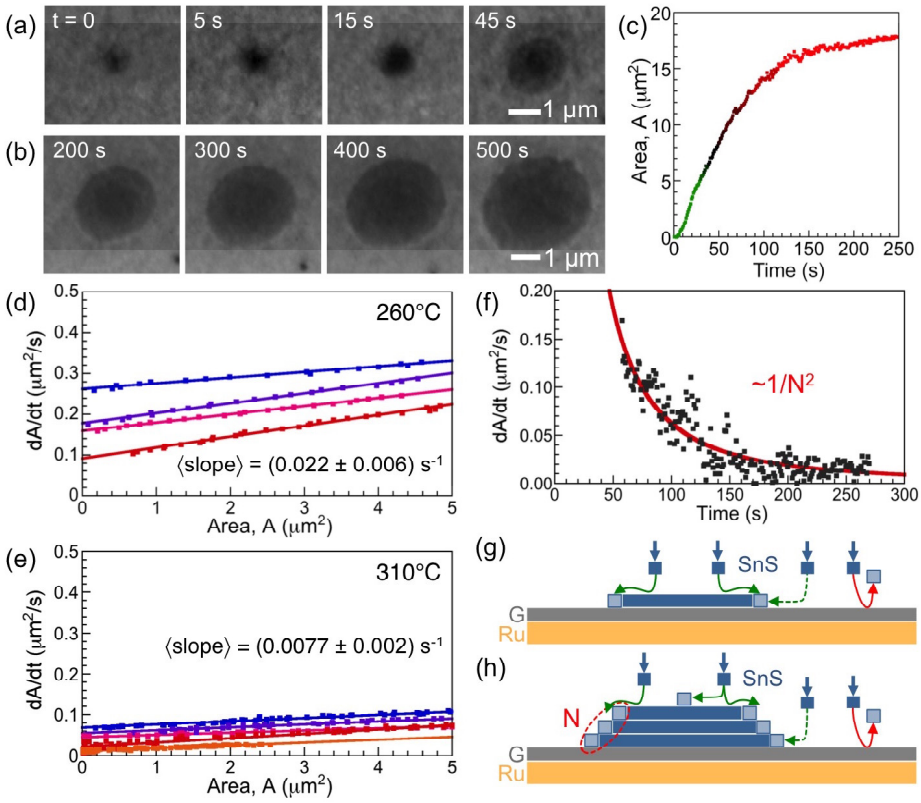

Figure 4: Analysis of SnS growth on MLG/Ru(0001) vdW support. (a) LEEM image sequence showing the nucleation and initial growth (up to 45s after nucleation) of a single SnS island on graphene/Ru at 260°C. **(b)** Late-stage growth of the same SnS flake. Note the nearly circular (isotropic) shape. Electron energy: ε = 5.8 eV. **(c)** Analysis of the projected area versus elapsed time from the initial nucleation. Nearly all analyzed nuclei showed the same general growth behavior, a transition from supralinear behavior (green) to a late-stage saturation regime (red). **(d)** Plot of the growth rate (dA/dt) as a function of projected area, A, for four SnS flakes growing at 260°C. **(e)** Plot of (dA/dt) as a function of A for six SnS flakes growing at 310°C. **(f)** Plot of growth rate (dA/dt) as a function of time at late stages (transition to saturation regime in c, symbols), and fit assuming an increasing number of closely bunched steps (N) in the edges of the SnS flakes. **(g)** Schematic representation of the capture of SnS from the vapor phase at the early growth stage, and **(h)** at the late growth stage, where the flakes are bounded by steep sidewalls consisting of N bunched steps.

To analyze SnS growth on MLG/Ru and compare with growth on graphite, we again followed the lateral expansion of individual SnS flakes in real-time movies obtained during MBE growth. The analysis of such data is shown in Figure 4. Following the initial nucleation, SnS flakes expand continuously both at the early stage (Fig. 4a) and at later stages of their growth (Fig. 4b). Measurements of the time-dependent lateral growth invariably show an early, supralinear behavior transitioning into a saturation regime at longer times (see Fig. 4c). Our analysis of the early stage growth for two different substrate temperatures, 260°C and 310°C, is shown in Fig. 4d and Fig. 4e, respectively. Similar to growth on graphite (Fig. 2c), the lateral growth rate in both cases is proportional to the projected flake area A. For identical flux from the MBE source, the rate increases substantially (~3 times) faster with area at the lower sample temperature, which is consistent with the expected increase in SnS sticking coefficient at lower temperatures. Most importantly, however, the growth rates no longer tend to zero for $A \rightarrow 0$. The finite intercept, *i.e.*, the finite rate dA/dt for A = 0 implies that on MLG/Ru substrates, SnS no longer condenses primarily on the surface of SnS islands but a significant supply of SnS now stems from adsorption on the surrounding substrate (Fig. 4g). The slowing of the lateral expansion rate at later stages (Fig. 4c) is rationalized in Fig. 4f, which compares the measured time dependence of dA/dt with a fit assuming that the flake edges comprise bunches of atomic steps whose size increases continuously due to the addition of layers during vertical growth. As the size of the edge step-bunches increases the growth flux is progressively divided among a larger number of steps (N), with the effect of slowing lateral growth (Fig. 4h). While possible step-crossing barriers[41-42] for adsorbed SnS could have similar effects, the measured dA/dt at late stages fits perfectly to the expected $1/N^2$ behavior for incorporation of SnS into growing step bunches. The slowing lateral growth will ultimately limit the achievable footprint of single

crystalline islands and may prevent coalescence to continuous films in SnS growth on vdW substrates (saturation regime, Figs. 4c, f).

Comparing SnS growth on graphite (Figure 2) and on graphene/Ru (Figures 3, 4), we conclude that the negligible SnS adsorption on graphite and the enhanced reactivity and resulting increased adsorption of SnS vapor on MLG/Ru cause key differences between the two vdW supports. On MLG/Ru the supply of SnS not only from existing SnS nuclei but also from the nearby substrate causes substantially enhanced lateral growth (and hence larger lateral size of the nuclei) as well as nearly isotropic in-plane shapes of the nuclei compared to the faceted shapes observed on graphite. This suggests a likely kinetic origin of the rectangular SnS island shapes on graphite, either due to anisotropic surface diffusion along and across the ridges of the topmost SnS sheet or as a result of different step-crossing barriers.

In the few-layer growth realized here, we used *in-situ* microscopy to identify other mechanisms of layered crystal growth that differ from those of conventional 3D solids. One key difference lies in the ways defects such as dislocations are accommodated. In 3D crystals, dislocations either form closed loops or terminate at a free surface.[43] In layered crystals the weak interlayer coupling implies that dislocations can also end at any of the internal vdW interfaces. The tendency of these crystals to form growth spirals or pyramids,[44] centered around screw dislocations, has long been noted.[45] Such structures are important since they further facilitate vertical growth by enabling the addition of layers without the need for nucleation. In addition, screw dislocations have recently been predicted to display unique spin textures with possibly higher degrees of spin coherency than the conventional Rashba-Dresselhaus spin-orbit coupling.[46] The competition between net growth and sublimation, which

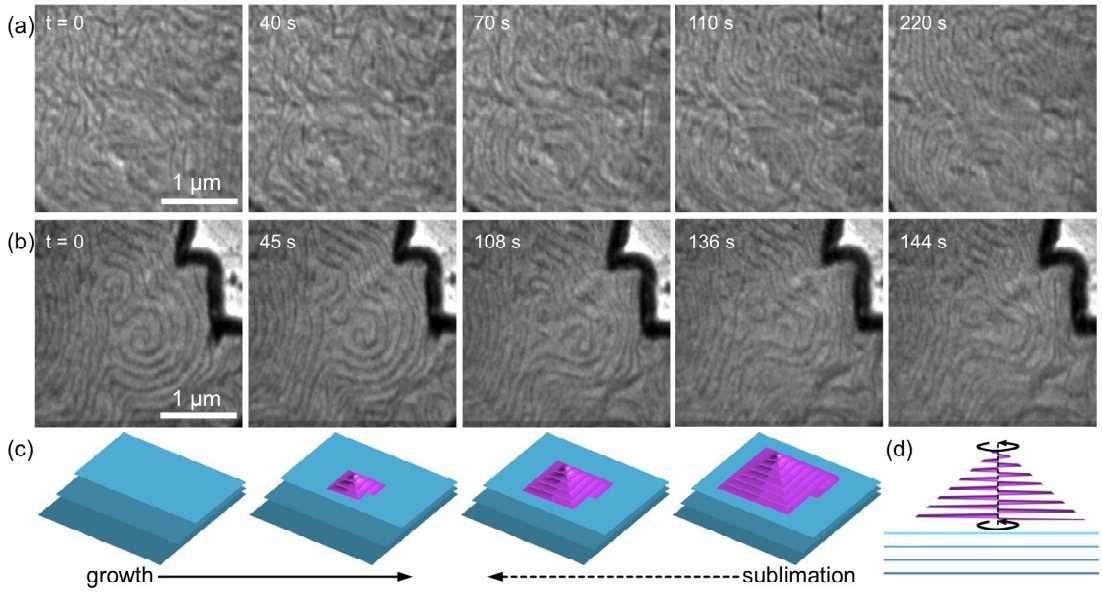

Figure 5: Spiral growth of layered SnS. (a) Sequence of LEEM images obtained during SnS deposition at 280°C, showing an initially stepped surface (dark lines – atomic steps) that accommodates the formation of several growth spirals centered at screw dislocations. **(b)** LEEM image sequence obtained during SnS sublimation at 330°C, showing the decay of a large growth spiral through inverse step flow. **(c)** Schematic showing the formation or decay of a growth spiral on a defect-free (stepped) layered crystal surface. **(d)** Side view showing how screw dislocations can terminate at the free surface or at an internal vdW interface in a layered crystal.

for constant deposition flux from the SnS evaporator is easily adjusted by small changes in substrate temperature, can be used to observe the initiation and annihilation of screw dislocations in SnS. Real-time microscopy in the growth regime shows that few-layer SnS with stepped surfaces readily transitions to spiral growth centered at screw dislocations introduced on the defect-free crystal surface (Fig. 5a; supporting movie S4). Conversely, as the substrate temperature is increased to initiate net sublimation from the sample, SnS removal from the growth spirals can cause the complete elimination of screw dislocations and restore a defect free remaining crystal (Fig. 5b; supporting movie S5). These observations of reversible spiral growth on few-layer SnS (shown schematically in Fig. 5c, d) are distinct from other spiral growth modes, for example spirals formed by pinning at substrate step edges in the early growth stages of Bi_2Se_3[47] or MoS_2[48] on graphene/SiC(0001). The combination of a sizable bandgap, high-Z constituents (Sn: Z = 50), and facile formation of screw dislocations make

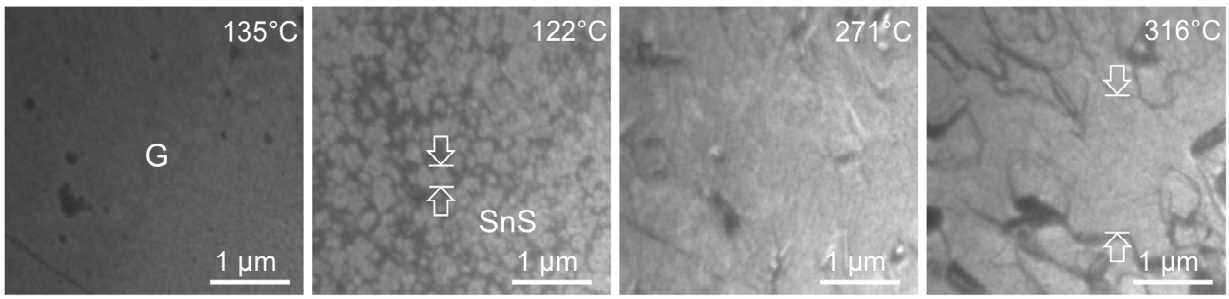

Figure 6: Rapid lateral grain growth in layered SnS. Sequence of LEEM images obtained during two-step SnS growth on graphite. Initial nucleation at ~120°C results in a dense array of small single-crystalline nuclei (size < 250 nm). The temperature was then raised and additional SnS deposited between 270°C and 320°C. The additional SnS dose, estimated by following the flow of atomic steps to ~50 atomic layers, causes lateral grain growth to sizes well beyond 1.5 µm, about 6 times the size of the initial nuclei.

few-layer SnS an interesting system for realizing novel helical 1D spin-current channels at screw dislocations.[46]

Aside from the unique properties predicted for monolayer sheets, thicker (bulk-like) layers of group IV monochalcogenide semiconductors, such as Ge(S, Se) or Sn(S, Se) are of broad interest for applications in thin film photovoltaics[2-7] and thermoelectrics,[8] among others. We conclude by discussing how our results from *in-situ* microscopy can guide efforts to grow high-quality multilayer films for these applications. Firstly, a well-defined film texture, such as a uniform *c*-axis orientation with layering parallel to the substrate, is desirable for many applications and is clearly achieved by MBE growth on vdW supports. Furthermore, compact films with large sizes of the individual single-crystalline grains are often required. The progressive slowing of the in-plane growth rate of SnS grains observed in our experiments implies an intrinsic limit to the achievable lateral grain size, which on graphite is ~1 µm but for growth on graphene/Ru approaches ~10 µm (Fig. S2). To obtain compact films, our results suggest a two-step process with nucleation at low temperature to seed the surface with an array of small grains followed by grain growth at higher temperature. We note here another fundamental difference between layered materials and conventional 3D crystal, namely the

rapid lateral grain growth in layered crystals. In 3D crystals, grains with fast-growing surface facets can kinetically outgrow misoriented grains so as to ultimately develop a microstructure with a specific texture,[49-50] which develops gradually over a significant thickness of a growing film. In layered crystals on the other hand, due to the weak interlayer interaction and hence small energy penalty associated with twisted stacking,[51] a nucleus with rapid lateral growth can readily expand across many underlying misoriented grains. This greatly facilitates lateral grain growth in layered crystals, which in the ultimate limit can occur during the addition of a single atomic sheet. Hence, a small-grain nucleation layer initiated at low temperature can easily be overgrown by much larger sheets to obtain high-quality continuous films with large grain size (Figure 6).

To document the quality of such few-layer and multilayer SnS flakes and films we

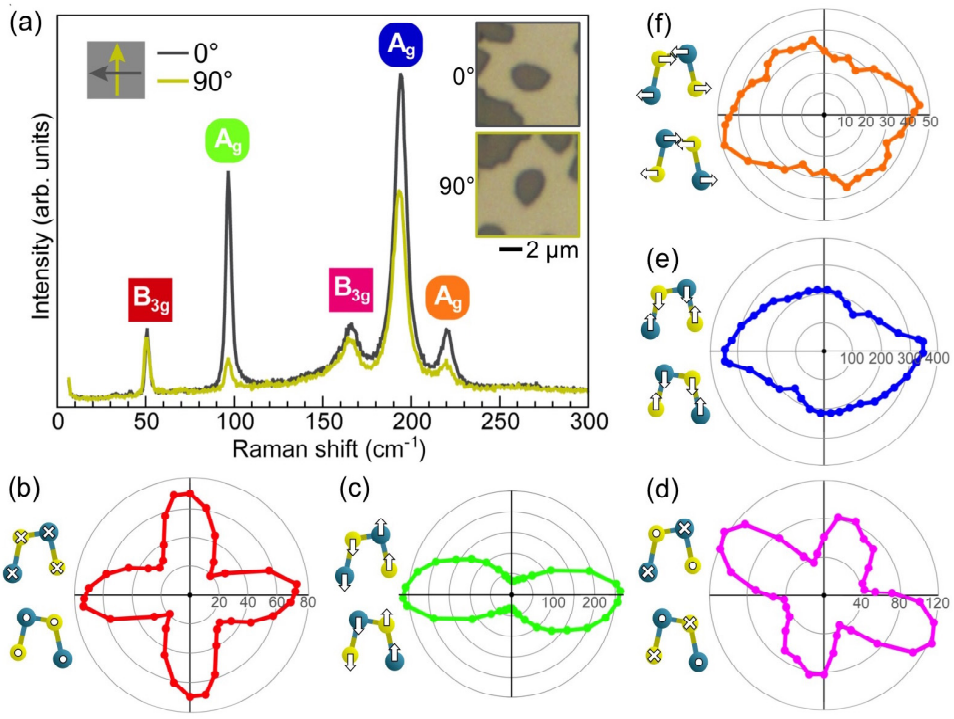

Figure 7: Anisotropic properties of basal-plane oriented, orthorhombic SnS. (a) Raman spectra of a SnS flake obtained with 0° and 90° orientations of the linear polarization of the incident laser light. The inset shows optical images of the measured flake at 0° and 90° rotation. **(b)-(f)** Polar plots of Raman intensity as a function of incident laser polarization for the B_{3g} and A_g modes shown in (a). Insets in each panel show the atomic displacements in the different Raman active modes.

performed measurements including Raman and photoluminescence (PL) spectroscopy. Raman spectroscopy excited by linearly polarized laser light was used to confirm anisotropic properties[27-28] in our large-grain *c*-axis oriented SnS films. Spectra were collected at different sample rotation on individual monocrystalline SnS grains (as shown in Fig. 7a, inset). Examples for 0° and 90° rotation angle along with polar plots of the B_{3g} and A_g mode intensities are shown in Figure 7. All major Raman active modes are sensitive to the polarization of the incident radiation, and show four-fold (B_{3g}) and two-fold symmetry (A_g), respectively.[27-28] Furthermore, the SnS films exhibit strong room temperature PL with a pronounced emission maximum at 1.32 eV photon energy corresponding to band-to-band radiative recombination across the direct gap, as well as several higher energy emissions (Fig. S3).[19] Raman line scans (Fig. S4a, b) show intensity variations in both B_{3g} and A_g modes between thin and thicker SnS, but close inspection and comparison with polarization dependent Raman spectroscopy (Fig. 7) suggests that these changes may be primarily due to different SnS orientations in different areas probed by the line scan. PL shows systematic changes in relative intensity of the band-edge and higher energy emissions between areas of thin and thick SnS, with the lowest-energy (band-edge) luminescence consistently carrying larger spectral weight in thinner SnS (Fig. S4c). A detailed analysis of the light emission from our high-quality basal-plane oriented SnS films requires further work and is beyond the scope of this paper.

Conclusions

In conclusion, we have used real-time *in-situ* microscopy to probe the fundamental growth mechanisms of SnS, representative of the broader family of group IV monochalcogenides, on carbon-based van der Waals substrates. We find that an unusual disparity between a strongly favored SnS adsorption on the growing nuclei and much lower precursor sticking on the substrate – which is very large for growth on graphite but is reduced

on monolayer graphene on Ru(0001) – favors vertical growth and is the most important characteristic making it challenging to obtain large monolayer domains. An additional factor toward the preferred out-of-plane growth is the facile introduction of screw dislocations, since the resulting growth spirals enable nucleation-free, continuous growth in thickness. Since SnS shows similar chemical properties, congruent sublimation from powders,[52] etc., as other members of the same class of materials (*e.g.*, SnSe, GeS, GeSe), our findings can inform efforts to identify conditions for the scalable growth of single-layer sheets of different group IV monochalcogenide semiconductors, and they should also apply to other layered/2D crystals with more open (*i.e.*, reactive) surfaces than the well-studied transition metal dichalcogenides. Besides ultrathin layers, our results also guide the synthesis of thicker films. SnS films achieved on a monolayer graphene/Ru van der Waals substrate show properties, such as uniform *c*-axis orientation, large size of the individual single-crystalline grains, anisotropic Raman scattering, and strong room temperature photoluminescence, that make them interesting for a wide range of potential applications, for example in the emission or detection of polarized light or in energy conversion processes, including thin film and third generation bulk (shift-current) photovoltaics.

Materials and Methods

In-situ microscopy and complementary selected-area low-energy electron diffraction (Micro-LEED) were performed in an Elmitec LEEM III low-energy electron microscope (LEEM) that allows observations at variable temperature (room temperature to ~1200°C) in ultrahigh vacuum (UHV) as well as during exposure of the samples to gases or vapors with ~6 nm lateral and monolayer height resolution. The instrument was modified extensively to enable microscopy of chalcogenide growth and accommodate exposure to sulfur and selenium rich

conditions. Bright-field LEEM at incident electron energies between ~1-6 eV was used to observe the growth processes in real time. Graphite substrates were prepared by mechanical cleavage, followed by degassing at ~350°C in UHV. Monolayer graphene/Ru(0001) substrates were prepared *in-situ* by exposure of samples of epitaxial Ru(0001) on sapphire (Al_2O_3(0001))[39-40] to ethylene at temperatures of 800-850°C. Sample temperatures were measured using a W-Re thermocouple spot-welded onto the sample support. Gas pressures were measured using a hot-filament ionization gauge. SnS was congruently evaporated (*i.e.*, by sublimation of intact SnS formula units)[53] using a custom-built miniature Knudsen MBE cell while recording the resulting growth on the surface in real time by bright-field LEEM. For additional *ex-situ* characterization, we performed optical microscopy, micro-Raman, and PL spectroscopy and mapping in a Horiba XPlora Plus microscope with excitation by a linearly polarized laser at 532 nm wavelength and a power of ~0.1 mW. Polarization-dependent Raman spectra were measured on individual single-crystalline SnS flakes through stepwise reorientation of the sample on a precision rotation stage. Scanning electron microscopy (SEM) of SnS grown on other substrates (Au/SiO_2, and SiO_2/Si; Fig. 1) were obtained in a FEI Helios instrument at an electron energy of 3 keV.

Acknowledgements

This work was supported by the U.S. Department of Energy, Office of Science, Basic Energy Sciences, under Award No. DE-SC0016343. The authors acknowledge technical support by J. Wang and G. Zhou.

Supporting Information. *Supporting figures (Figs. S1-S4):* Preparation of graphite and monolayer graphene/Ru(0001) starting substrates; optical microscopy of SnS films; photoluminescence and Raman spectra. *Supporting movies (Movies S1-S5):* SnS growth on

graphite; SnS growth on graphene/Ru(0001); SnS growth by incorporation into layer edges; onset of spiral growth; spiral decomposition during SnS sublimation.

References

1. Gomes, L. C.; Carvalho, A. Phosphorene Analogues: Isoelectronic Two-Dimensional Group-IV Monochalcogenides with Orthorhombic Structure. *Physical Review B* **2015**, *92*, 085406.
2. Engelken, R. D.; McCloud, H. E.; Lee, C.; Slayton, M.; Ghoreishi, H. Low Temperature Chemical Precipitation and Vapor Deposition of Sn_xS Thin Films. *Journal of The Electrochemical Society* **1987**, *134*, 2696-2707.
3. Mishra, K.; Rajeshwar, K.; Weiss, A.; Murley, M.; Engelken, R. D.; Slayton, M.; McCloud, H. E. Electrodeposition and Characterization of SnS Thin Films. *Journal of The Electrochemical Society* **1989**, *136*, 1915-1923.
4. Steinmann, V.; Jaramillo, R.; Hartman, K.; Chakraborty, R.; Brandt, R. E.; Poindexter, J. R.; Lee, Y. S.; Sun, L.; Polizzotti, A.; Park, H. H.; Gordon, R. G.; Buonassisi, T. 3.88% Efficient Tin Sulfide Solar Cells using Congruent Thermal Evaporation. *Advanced Materials* **2014**, *26*, 7488-7492.
5. Sinsermsuksakul, P.; Sun, L.; Lee, S. W.; Park, H. H.; Kim, S. B.; Yang, C.; Gordon, R. G. Overcoming Efficiency Limitations of SnS-Based Solar Cells. *Advanced Energy Materials* **2014**, *4*, 1400496.
6. Banai, R. E.; Horn, M. W.; Brownson, J. R. S. A Review of Tin(II) Monosulfide and its Potential as a Photovoltaic Absorber. *Solar Energy Materials and Solar Cells* **2016**, *150*, 112-129.
7. Burton, L. A.; Colombara, D.; Abellon, R. D.; Grozema, F. C.; Peter, L. M.; Savenije, T. J.; Dennler, G.; Walsh, A. Synthesis, Characterization, and Electronic Structure of Single-Crystal SnS, Sn2S3, and SnS2. *Chemistry of Materials* **2013**, *25*, 4908-4916.
8. Zhao, L.-D.; Lo, S.-H.; Zhang, Y.; Sun, H.; Tan, G.; Uher, C.; Wolverton, C.; Dravid, V. P.; Kanatzidis, M. G. Ultralow Thermal Conductivity and High Thermoelectric Figure of Merit in SnSe Crystals. *Nature* **2014**, *508*, 373-377.
9. Tuttle, B. R.; Alhassan, S. M.; Pantelides, S. T. Large Excitonic Effects in Group-IV Sulfide Monolayers. *Physical Review B* **2015**, *92*, 235405.
10. Xu, L.; Yang, M.; Wang, S. J.; Feng, Y. P. Electronic and Optical Properties of the Monolayer Group-IV Monochalcogenides MX (M = Ge, Sn; X = S, Se, Te). *Physical Review B* **2017**, *95*, 235434.
11. Li, F.; Liu, X.; Wang, Y.; Li, Y. Germanium Monosulfide Monolayer: A Novel Two-Dimensional Semiconductor with a High Carrier Mobility. *Journal of Materials Chemistry C* **2016**, *4*, 2155-2159.
12. Peng, L.; Wang, C.; Qian, Q.; Bi, C.; Wang, S.; Huang, Y. Complete Separation of Carriers in the GeS/SnS Lateral Heterostructure by Uniaxial Tensile Strain. *ACS Applied Materials & Interfaces* **2017**, *9*, 40969-40977.
13. Hanakata, P. Z.; Carvalho, A.; Campbell, D. K.; Park, H. S. Polarization and Valley Switching in Monolayer Group-IV Monochalcogenides. *Physical Review B* **2016**, *94*, 035304.

14. Wu, M.; Zeng, X. C. Intrinsic Ferroelasticity and/or Multiferroicity in Two-Dimensional Phosphorene and Phosphorene Analogues. *Nano Letters* **2016**, *16*, 3236-3241.

15. Fei, R.; Li, W.; Li, J.; Yang, L. Giant Piezoelectricity of Monolayer Group IV Monochalcogenides: SnSe, SnS, GeSe, and GeS. *Applied Physics Letters* **2015**, *107*, 173104.

16. Hua, W.; Xiaofeng, Q. Two-Dimensional Multiferroics in Monolayer Group IV Monochalcogenides. *2D Materials* **2017**, *4*, 015042.

17. Kushnir, K.; Wang, M.; Fitzgerald, P. D.; Koski, K. J.; Titova, L. V. Ultrafast Zero-Bias Photocurrent in GeS Nanosheets: Promise for Photovoltaics. *ACS Energy Letters* **2017**, *2*, 1429-1434.

18. Sutter, E.; Huang, Y.; Komsa, H. P.; Ghorbani-Asl, M.; Krasheninnikov, A. V.; Sutter, P. Electron-Beam Induced Transformations of Layered Tin Dichalcogenides. *Nano Letters* **2016**, *16*, 4410-4416.

19. Sutter, P.; Komsa, H.-P.; Krasheninnikov, A. V.; Huang, Y.; Sutter, E. Luminescence of Defects in the Structural Transformation of Layered Tin Dichalcogenides. *Applied Physics Letters* **2017**, *111*, 262102.

20. Steinmann, V.; Chakraborty, R.; Rekemeyer, P. H.; Hartman, K.; Brandt, R. E.; Polizzotti, A.; Yang, C.; Moriarty, T.; Gradečak, S.; Gordon, R. G.; Buonassisi, T. A Two-Step Absorber Deposition Approach To Overcome Shunt Losses in Thin-Film Solar Cells: Using Tin Sulfide as a Proof-of-Concept Material System. *ACS Applied Materials & Interfaces* **2016**, *8*, 22664-22670.

21. Jamali-Sheini, F.; Cheraghizade, M.; Yousefi, R. SnS Nanosheet Films Deposited via Thermal Evaporation: The Effects of Buffer Layers on Photovoltaic Performance. *Solar Energy Materials and Solar Cells* **2016**, *154*, 49-56.

22. Patel, M.; Kim, H.-S.; Kim, J. Wafer-Scale Production of Vertical SnS Multilayers for High-Performing Photoelectric Devices. *Nanoscale* **2017**, *9*, 15804-15812.

23. Revathi, N.; Bereznev, S.; Iljina, J.; Safonova, M.; Mellikov, E.; Volobujeva, O. PVD Grown SnS Thin Films onto Different Substrate Surfaces. *Journal of Materials Science: Materials in Electronics* **2013**, *24*, 4739-4744.

24. Mutlu, Z.; Wu, R. J.; Wickramaratne, D.; Shahrezaei, S.; Liu, C.; Temiz, S.; Patalano, A.; Ozkan, M.; Lake, R. K.; Mkhoyan, K. A.; Ozkan, C. S. Phase Engineering of 2D Tin Sulfides. *Small* **2016**, *12*, 2998-3004.

25. Wangperawong, A.; Herron, S. M.; Runser, R. R.; Hägglund, C.; Tanskanen, J. T.; Lee, H.-B.-R.; Clemens, B. M.; Bent, S. F. Vapor Transport Deposition and Epitaxy of Orthorhombic SnS on Glass and NaCl Substrates. *Applied Physics Letters* **2013**, *103*, 052105.

26. Wang, S. F.; Fong, W. K.; Wang, W.; Surya, C. Growth of Highly Textured SnS on Mica using an SnSe Buffer Layer. *Thin Solid Films* **2014**, *564*, 206-212.

27. Tian, Z.; Guo, C.; Zhao, M.; Li, R.; Xue, J. Two-Dimensional SnS: A Phosphorene Analogue with Strong In-Plane Electronic Anisotropy. *ACS Nano* **2017**, *11*, 2219-2226.

28. Li, M.; Wu, Y.; Li, T.; Chen, Y.; Ding, H.; Lin, Y.; Pan, N.; Wang, X. Revealing Anisotropy and Thickness Dependence of Raman Spectra for SnS Flakes. *RSC Advances* **2017**, *7*, 48759-48765.

29. Xiang, Y.; Yang, Y.; Guo, F.; Sun, X.; Lu, Z.; Mohanty, D.; Bhat, I.; Washington, M.; Lu, T.-M.; Wang, G.-C. Van der Waals Epitaxy of SnS Film on Single Crystal Graphene Buffer Layer on Amorphous SiO_2/Si. *Applied Surface Science* **2018**, *435*, 759-768.

30. Wang, W.; Leung, K.; Fong, W.; Wang, S.; Hui, Y.; Lau, S.; Chen, Z.; Shi, L.; Cao, C.; Surya, C. Molecular Beam Epitaxy Growth of High Quality p-Doped SnS Van der Waals Epitaxy on a Graphene Buffer Layer. *Journal of Applied physics* **2012**, *111*, 093520.

31. Sutter, P. W.; Flege, J.-I.; Sutter, E. A. Epitaxial Graphene on Ruthenium. *Nature Materials* **2008**, *7*, 406-411.

32. Sutter, P.; Lahiri, J.; Albrecht, P.; Sutter, E. Chemical Vapor Deposition and Etching of High-Quality Monolayer Hexagonal Boron Nitride Films. *ACS Nano* **2011**, *5*, 7303-7309.

33. Li, B.; Gong, Y.; Hu, Z.; Brunetto, G.; Yang, Y.; Ye, G.; Zhang, Z.; Lei, S.; Jin, Z.; Bianco, E.; Zhang, X.; Wang, W.; Lou, J.; Galvão, D. S.; Tang, M.; Yakobson, B. I.; Vajtai, R.; Ajayan, P. M. Solid–Vapor Reaction Growth of Transition-Metal Dichalcogenide Monolayers. *Angewandte Chemie International Edition* **2016**, *55*, 10656-10661.

34. Burton, L. A.; Walsh, A. Phase Stability of the Earth-Abundant Tin Sulfides SnS, SnS_2, and Sn_2S_3. *The Journal of Physical Chemistry C* **2012**, *116*, 24262-24267.

35. Jizhou, J.; Calvin Pei Yu, W.; Jing, Z.; Shisheng, L.; Qixing, W.; Jianyi, C.; Dianyu, Q.; Hongyu, W.; Goki, E.; Daniel, H. C. C.; Yumeng, S.; Wenjing, Z.; Andrew Thye Shen, W. Two-Step Fabrication of Single-Layer Rectangular SnSe Flakes. *2D Materials* **2017**, *4*, 021026.

36. Sutter, E.; Albrecht, P.; Wang, B.; Bocquet, M.-L.; Wu, L.; Zhu, Y.; Sutter, P. Arrays of Ru Nanoclusters with Narrow Size Distribution Templated by Monolayer Graphene on Ru. *Surface Science* **2011**, *605*, 1676-1684.

37. Zhou, H.; Zhang, L.; Mao, J.; Li, G.; Zhang, Y.; Wang, Y.; Du, S.; Hofer, W. A.; Gao, H.-J. Template-Directed Assembly of Pentacene Molecules on Epitaxial Graphene on Ru(0001). *Nano Research* **2013**, *6*, 131-137.

38. Yang, K.; Xiao, W. D.; Jiang, Y. H.; Zhang, H. G.; Liu, L. W.; Mao, J. H.; Zhou, H. T.; Du, S. X.; Gao, H. J. Molecule–Substrate Coupling between Metal Phthalocyanines and Epitaxial Graphene Grown on Ru(0001) and Pt(111). *The Journal of Physical Chemistry C* **2012**, *116*, 14052-14056.

39. Sutter, P. W.; Albrecht, P. M.; Sutter, E. A. Graphene Growth on Epitaxial Ru Thin Films on Sapphire. *Applied Physics Letters* **2010**, *97*, 213101.

40. Sutter, P.; Ciobanu, C. V.; Sutter, E. Real-Time Microscopy of Graphene Growth on Epitaxial Metal Films: Role of Template Thickness and Strain. *Small* **2012**, *8*, 2250.

41. Ehrlich, G.; Hudda, F. G. Atomic View of Surface Self-Diffusion: Tungsten on Tungsten. *The Journal of Chemical Physics* **1966**, *44*, 1039-1049.

42. Schwoebel, R. L.; Shipsey, E. J. Step Motion on Crystal Surfaces. *Journal of Applied Physics* **1966**, *37*, 3682-3686.

43. Hirth, J. P.; Lothe, J., *Theory of Dislocations*. 2nd ed.; Wiley: New York, 1982.

44. Burton, W. K.; Cabrera, N.; Frank, F. C. The Growth of Crystals and the Equilibrium Structure of their Surfaces. *Philosophical Transactions of the Royal Society, London* **1951**, *243*, 299-358.

45. Bletskan, D. I.; Budyanskii, V. I.; Kopinets, I. F.; Mikulaninets, S. V. Photoelectric Properties of Single Crystals of GeS Obtained from the Gas Phase. *Inorganic Materials* **1976**, *12*, 202.

46. Hu, L.; Huang, H.; Wang, Z.; Jiang, W.; Ni, X.; Zhou, Y.; Zielasek, V.; Lagally, M. G.; Huang, B.; Liu, F. Ubiquitous Ideal Spin-Orbit Coupling in a Screw Dislocation in Semiconductors. *arXiv:1801.09025 [cond-mat.mtrl-sci]* **2018**.

47. Liu, Y.; Weinert, M.; Li, L. Spiral Growth without Dislocations: Molecular Beam Epitaxy of the Topological Insulator Bi_2Se_3 on Epitaxial Graphene/SiC(0001). *Physical Review Letters* **2012**, *108*, 115501.

48. Dong, X.; Yan, C.; Tomer, D.; Li, C. H.; Li, L. Spiral Growth of Few-Layer MoS_2 by Chemical Vapor Deposition. *Applied Physics Letters* **2016**, *109*, 051604.

49. Nokinov, V., *Grain Growth and Control of Microstructure and Texture in Polycrystalline Materials*. CRC: Boca Raton, 1997.

50. Thompson, C. V.; Carel, R. Texture Development in Polycrystalline Thin Films. *Materials Science and Engineering: B* **1995**, *32*, 211-219.

51. Liu, K.; Zhang, L.; Cao, T.; Jin, C.; Qiu, D.; Zhou, Q.; Zettl, A.; Yang, P.; Louie, S. G.; Wang, F. Evolution of Interlayer Coupling in Twisted Molybdenum Disulfide Bilayers. *Nature Communications* **2014**, *5*, 4966.

52. Sutter, E.; Sutter, P. 1D Wires of 2D Layered Materials: Germanium Sulfide Nanowires as Efficient Light Emitters. *ACS Applied Nano Materials* **2018**, *1*, 1042–1049.

53. Mills, K. C., *Thermodynamic Data for Inorganic Sulphides, Selenides and Tellurides*. Butterworths: London, 1974.

TOC Graphic

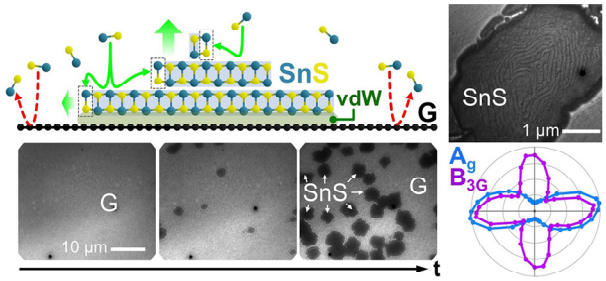

Supporting Information

Growth Mechanisms of Anisotropic Layered Group IV Chalcogenides on van der Waals Substrates for Energy Conversion Applications

Peter Sutter[1,*] and Eli Sutter[2]

[1]Department of Electrical and Computer Engineering, University of Nebraska-Lincoln, Lincoln, NE 68588, United States; [2]Department of Mechanical and Materials Engineering, University of Nebraska-Lincoln, Lincoln, NE 68588, United States

*Corresponding author, e-mail: psutter@unl.edu.

Supporting Figures

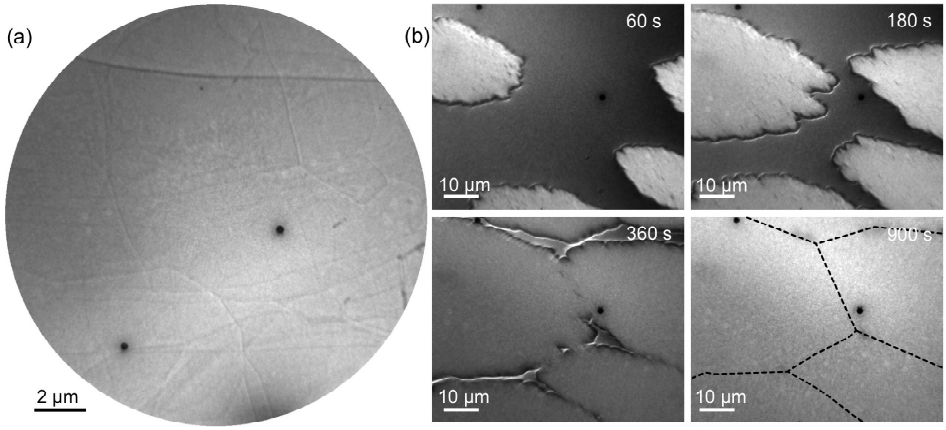

Figure S1: Van der Waals substrates used in this work. (a) Low-energy electron microscopy (LEEM) image of the starting graphite (HOPG) surface prepared by mechanical exfoliation followed by degassing in ultrahigh-vacuum. **(b)** Growth of monolayer graphene on Ru(0001) by exposure to ethylene at high temperature. The LEEM image series shows sparse nucleation of graphene, which translates into large domain size and correspondingly low density of domain boundaries, which are the primary defects in high-quality graphene/Ru(0001) films. Temperature: 840°C.

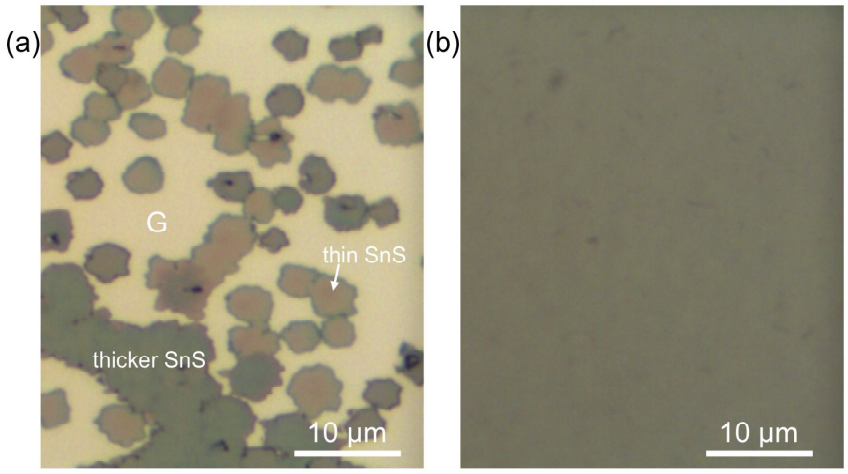

Figure S2: Partially and fully coalesced basal-plane oriented SnS film on monolayer graphene/Ru(0001). (a) Optical micrograph showing the morphology and size of single-crystalline SnS domains at partial surface coverage. **(b)** Optical micrograph at full surface coverage of coalesced SnS, which forms a dense layer with uniform thickness and basal-plane orientation.

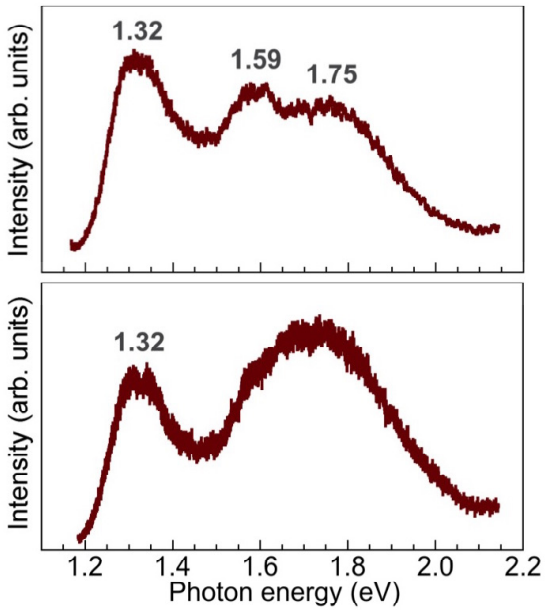

Figure S3: Photoluminescence (PL) spectroscopy of high-quality basal-plane oriented SnS grown on a graphene/Ru vdW substrate. Typical room temperature PL spectra obtained on different samples, showing a characteristic emission at a photon energy hv = 1.32 eV, along with several higher energy transitions.

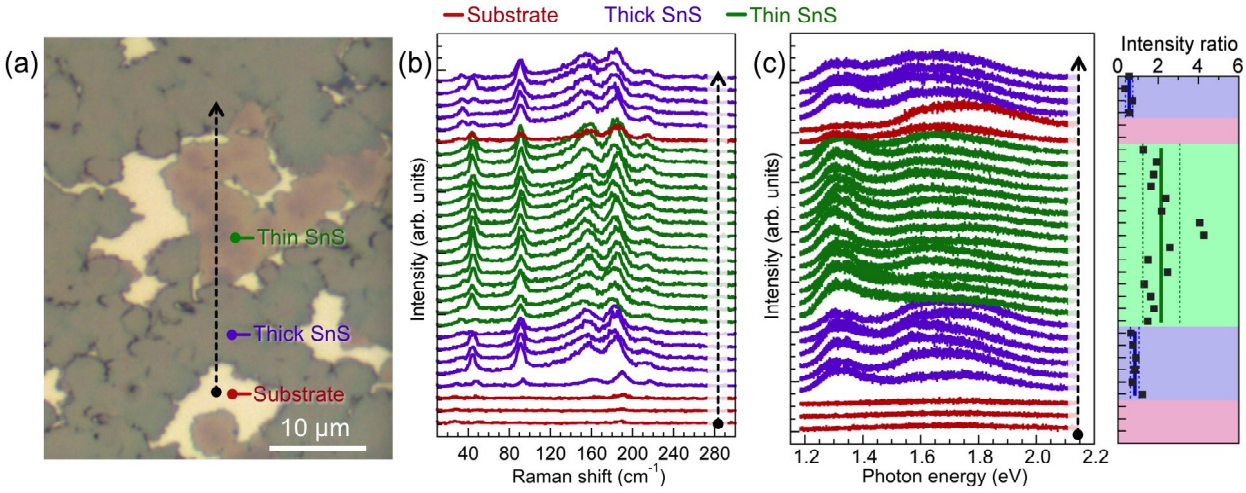

Figure S4: Raman and photoluminescence (PL) line scans across thick and thin SnS. (a) Optical micrograph of partially coalesced SnS grown on graphene/Ru. **(b)** Raman spectra measured along the line marked in (a). **(c)** PL spectra measured along the line marked in (a). The right-hand panel summarizes the analysis of the ratio of PL intensity between the band-edge peak (1.32 eV) and the broader peak at higher energy (1.6 – 1.8 eV), showing ~2 times higher intensity of the band-edge peak for thin SnS and intensity ratios below 1 for thicker SnS. Black symbols represent the measured data. Solid lines indicate the mean of all measured points in the same shaded region. Dashed lines represent $\pm 1\sigma$ (standard deviation). All measurements were performed at room temperature.

Supporting Movies (captions)

Movie S1: MBE growth of SnS on graphite at 260°C. Corresponding to the image sequence shown in Fig. 2 a. Real-time low-energy electron microscopy (LEEM) movie; original capture rate: 1 frame per second (every second frame is shown). Elapsed time is given in seconds.

Movie S2: SnS growth on monolayer graphene/Ru(0001) at 280°C. Corresponding to the image sequence shown in Fig. 3 a. Real-time LEEM movie, capture rate: 1 frame per second. Elapsed time is given in seconds. Electron energy ε = 5.8 eV.

Movie S3: Edge-flow growth of few-layer SnS on monolayer graphene/Ru(0001) at 280°C. Dark lines are edges of individual SnS atomic sheets. Real-time LEEM movie, capture rate: 1 frame per second. Elapsed time is given in min:sec. Electron energy ε = 2.6 eV.

Movie S4: Onset of spiral growth of few-layer SnS on monolayer graphene/Ru(0001) at 280°C. Dark lines are edges of individual SnS atomic sheets. Several growth spirals develop during the period captured by the movie. Real-time LEEM movie, capture rate: 1 frame per second. Elapsed time is given in seconds. Electron energy ε = 2.6 eV. Scale bar: 0.5 µm.

Movie S5: Spiral decomposition during sublimation of few-layer SnS on monolayer graphene/Ru(0001) at 330°C. Dark lines are edges of individual SnS atomic sheets, which retract in inverse edge-flow during sublimation from the surface. Growth spirals are eliminated due to materials removal by sublimation during the period captured by the movie. Real-time LEEM movie, capture rate: 1 frame per second. Elapsed time is given in seconds. Electron energy ε = 2.6 eV. Scale bar: 0.5 µm.